
AURORA: Autonomous Regularization for One-shot Representation Alignment

Anonymous Authors¹

Abstract

One-shot Federated Learning (OFL) pushes communication efficiency to its limit but suffers from severe model inconsistency under non-IID data. A natural remedy is to anchor local prototypes to a globally shared geometric structure (Simplex ETF). However, we discover that current state-of-the-art OFL methods fail catastrophically in extreme non-IID settings, with accuracy collapsing to <25% (e.g., DENSE at 20.5%, FedAvg at 15.6%) due to feature space misalignment. We identify a “Temporal Dichotomy”: geometric anchors are only effective when coupled with *dynamic* scheduling. Building on this discovery, we propose AURORA, a framework that *automates* this scheduling via gradient decoupling and meta-annealing. AURORA systematically outperforms baselines by up to 28% and surpasses manually-tuned schedules by 2.55% with significantly reduced variance (0.54 vs 1.31), turning a marginal improvement into dominant performance.

1. Introduction

Federated Learning (FL) has emerged as the de facto paradigm for collaborative machine learning under privacy constraints (McMahan et al., 2017). Despite its success, traditional multi-round FL suffers from prohibitive communication overhead, especially when deploying large-scale models over bandwidth-constrained edge networks. **One-shot Federated Learning (OFL)** pushes communication efficiency to its limit by restricting the client-server interaction to a single round (Guha et al., 2019). However, this “train-then-merge” paradigm faces a critical challenge: **Model Inconsistency** (Zeng et al.). Under Non-IID data distributions, local models optimizing solely for local tasks tend to drift into disparate regions of the feature space. Without periodic

¹Anonymous Institution, Anonymous City, Anonymous Region, Anonymous Country. Correspondence to: Anonymous Author <anon.email@domain.com>.

Preliminary work. Under review by the International Conference on Machine Learning (ICML). Do not distribute.

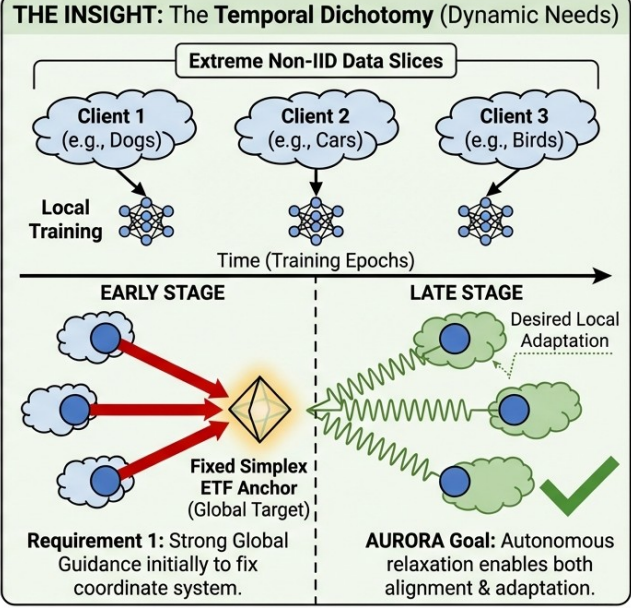
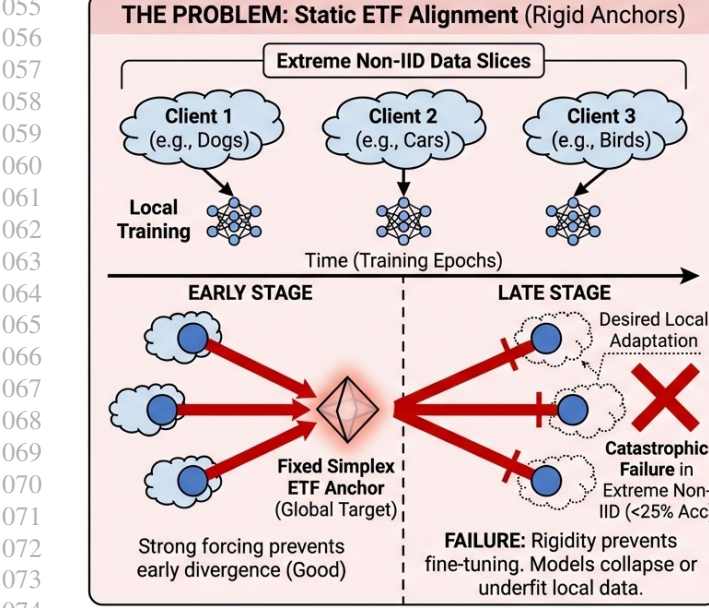
synchronization to correct these drifts, *parameter-space* aggregation methods (e.g., FedAvg) fail catastrophically due to the **permutation invariance** of deep networks—different clients learn functionally similar features at disparate neuron locations, causing layer collapse upon averaging. Similarly, recent analytic approaches like AFL (He et al., 2025), while promising for pre-trained models, fail to learn discriminative features from scratch in one-shot settings (see Table 1), highlighting the difficulty of the problem.

To address model inconsistency, recent advances such as FAFI (Zeng et al.) augment local training with contrastive learning. However, these methods lack *explicit global geometric anchors*. A natural remedy is to align client prototypes to a fixed Simplex Equiangular Tight Frame (ETF) structure (Papyan et al., 2020). However, we discover that **static alignment effectively hurts performance**, identifying a “**Temporal Dichotomy**”: the optimal balance between global alignment and local adaptation is *time-varying*. In the *early stage*, strong alignment prevents overfitting; in the *late stage*, relaxed alignment enables fine-grained adaptation. Static regularization fails to satisfy both needs, whereas AURORA automates this scheduling to achieve the best of both worlds without manual tuning.

To bridge this gap, we propose **AURORA** (Autonomous Uncertainty-based Regularization for One-shot Representation Alignment), a framework that *automates* the required dynamic scheduling. The key insight is *gradient decoupling*: rather than letting uncertainty weights directly scale model gradients (which causes training instability), we decouple the meta-objective to learn client-specific, data-dependent regularization trajectories. Combined with a monotonic meta-annealing prior and stability regularization, AURORA matches or exceeds manually-tuned baselines across CIFAR and SVHN using a *single fixed hyperparameter configuration*.

Our principal contributions are summarized as follows:

- **The Temporal Dichotomy:** We empirically identify and characterize the Temporal Dichotomy—showing why static geometric alignment fails in One-shot FL while dynamic scheduling succeeds.
- **AURORA Framework:** We propose gradient-decoupled uncertainty weighting with meta-annealing,



Challenge: How to autonomously transition from rigid anchoring to relaxed adaptation without manual tuning?

Figure 1. The Motivation: Visualizing the "Temporal Dichotomy" in One-Shot FL. (Left) The Failure of Static Alignment: While strictly anchoring local prototypes to a global ETF structure (large λ) prevents feature drift in the early stage, it becomes too rigid in the late stage, prohibiting necessary local adaptation and causing model collapse. (Right) The Dynamic Need: We identify that the optimal alignment strength is time-varying. A robust system requires strong global guidance initially to fix the coordinate system, followed by autonomous relaxation (green waves) to enable fine-grained feature learning. AURORA automates this trajectory without manual tuning.

enabling autonomous regularization trajectory learning without manual schedule tuning.

- **Robustness Mechanism:** We identify and address the “exploding λ ” failure mode in extreme non-IID scenarios through stability regularization.
- **Comprehensive Evaluation:** AURORA achieves state-of-the-art results across multiple benchmarks with a single hyperparameter configuration, eliminating per-dataset schedule search.

2. Related Work

2.1. One-shot Federated Learning and Non-IID Challenges

Data heterogeneity (Non-IID) poses severe challenges in One-shot FL (OFL) due to the lack of iterative correction (Amato et al., 2025). While multi-round methods like FedProx (Li et al., 2020) and SCAFFOLD (Karimireddy et al., 2020) address this via frequent communication, OFL requires robust single-round solutions. Existing approaches largely fall into three categories: (1) **Distillation-based** methods like DENSE (Zhang et al., 2022) and **Co-Boosting** (Dai et al.) simulate global data interactions. While Co-Boosting attempts to mitigate generator quality issues via adversarial hard-sample mining, our ex-

periments show it still suffers from generator mode collapse under extreme skew (achieving only 19.24% on CIFAR-100), as the disjoint ensemble cannot guide the generator effectively; (2) Aggregation-based methods like FedLPA (Liu et al., 2024) employ advanced Bayesian inference to weight parameters; however, as shown in our experiments, they struggle in one-shot settings with deep networks where permutation symmetries prevent substantial parameter alignment; and (3) Client-side enhancements like FAFI (Zeng et al.) focus on local feature quality. Recent work AFL (He et al., 2025) proposes an analytic approach for one-shot FL. However, AFL strictly relies on pre-trained frozen backbones to extract embeddings and solves a linear regression problem. As shown in our experiments, when applied to the standard FL setting (training from scratch) without pre-trained weights, AFL fails to learn discriminative features (20.10%), whereas AURORA successfully learns high-quality representations (48.83%) autonomously.

Progressive and Split Approaches: Recent works like FuseFL (Tang et al., 2024) attempt to break the isolation of local training by progressively fusing model blocks in a bottom-up manner. FuseFL views local training through a causal lens, arguing that feature augmentation from other clients removes spurious correlations. However, FuseFL strictly requires K sequential communication rounds (where K is the number of blocks), violating the strict single-

interaction constraint of OFL if $K > 1$. Furthermore, our experiments show that without a global coordinate system, progressive fusion struggles to align features under extreme label skew (CIFAR-100, $\alpha = 0.05$), achieving only 32.71% compared to AURORA’s 48.83%.

Unlike methods relying on complex auxiliary transmission (e.g., FALCON (Liu et al., 2026)) or server-side generation, AURORA purely regulates *local training dynamics* via geometric anchors to produce alignable models without extra communication overhead. Since AURORA relies on fixed ETF anchors, it also avoids prototype poisoning risks associated with dynamic prototype learning (Zeng et al., 2025).

2.2. Prototype-based Federated Learning and Neural Collapse

Prototype-based methods have gained traction for their communication efficiency. **FedProto** (Tan et al., 2022) exchanges class prototypes instead of model parameters. **FedTGP** (Zhang et al., 2024) introduces trainable global prototypes with adaptive-margin contrastive learning. Recent multi-round FL works have explored *adaptive prototype alignment weights* that vary across clients or training rounds; however, these methods rely on iterative server aggregation to correct alignment errors and are not applicable to the one-shot setting where clients train in isolation without feedback.

Our work leverages the *Neural Collapse* phenomenon (Papyan et al., 2020), which shows that optimal classifiers converge to a Simplex Equiangular Tight Frame (ETF) structure. **FedETF** (Li et al., 2023) utilizes fixed ETF classifiers to mitigate classifier bias in multi-round FL. In contrast, our approach addresses the **One-shot** regime where iterative synchronization is absent. Unlike FedETF’s focus on classifier-side weights, we introduce ETF anchors at the *prototype level* to provide a shared coordinate system for feature spaces across isolated clients.

Distinction from Prior Work. While FedETF (Li et al., 2023) uses fixed ETF structures in multi-round FL, and FAFI (Zeng et al.) enhances client-side training without geometric anchors, we are the first to investigate explicit geometric anchoring for **One-shot** prototype alignment. Critically, we discover that static alignment fails in OFL while dynamic scheduling succeeds (the “Temporal Dichotomy”)—a fundamental insight into why OFL behaves differently from multi-round FL. AURORA automates the required dynamic scheduling via gradient-based learning. Extended comparison in Appendix F.

2.3. Meta-Learning and Multi-Task Optimization

Our approach draws inspiration from multi-task learning research. **Kendall et al.** (Kendall et al., 2018) pioneered using homoscedastic uncertainty to automatically weight multi-task losses. **PCGrad** (Yu et al., 2020) addresses gradient conflicts through projection. **Franceschi et al.** (Franceschi et al., 2017) formalized gradient-based hyperparameter optimization via bilevel programming. AURORA can be viewed as an online, one-step approximation of bilevel optimization. **However, directly applying Kendall’s formulation to One-shot FL fails catastrophically (23.94% accuracy), as the implicit learning rate scaling destabilizes training. Our gradient decoupling mechanism is essential.**

3. The AURORA Framework: Autonomous Regularization

3.1. Preliminaries: The Dual Objectives in OFL

We consider a one-shot federated learning setting with K clients, each holding a private dataset \mathcal{D}_k drawn from a potentially distinct distribution. We extend FAFI’s formulation by introducing an explicit alignment loss:

$$\mathcal{L}_{\text{total}} = \mathcal{L}_{\text{local}} + \lambda \cdot \mathcal{L}_{\text{align}} \quad (1)$$

where:

- $\mathcal{L}_{\text{local}} = \mathcal{L}_{\text{cls}} + \mathcal{L}_{\text{con}} + \mathcal{L}_{\text{proto}}$ encompasses local supervision signals
- $\mathcal{L}_{\text{align}}$ is the global alignment loss that encourages the client’s learnable prototypes to align with a fixed global target

ETF Anchor for Global Alignment. Inspired by the Neural Collapse theory (Papyan et al., 2020), we define:

$$\mathcal{L}_{\text{align}} = \frac{1}{|\mathcal{C}_k|} \sum_{c \in \mathcal{C}_k} \|\mathbf{p}_c - \mathbf{a}_c\|^2 \quad (2)$$

where \mathcal{C}_k is the set of classes present in client k ’s local dataset, $\mathbf{p}_c \in \mathbb{R}^d$ is the learnable prototype for class c , and \mathbf{a}_c is the corresponding column of the pre-defined ETF anchor matrix $\mathbf{A} \in \mathbb{R}^{d \times C}$, satisfying:

$$\mathbf{A}^\top \mathbf{A} = \frac{C}{C-1} \left(\mathbf{I}_C - \frac{1}{C} \mathbf{1}_C \mathbf{1}_C^\top \right) \quad (3)$$

This mathematically optimal structure ensures maximum inter-class separation and provides a consistent geometric target for all clients.

Crucially, $\mathcal{L}_{\text{align}}$ is computed solely between learnable prototypes and fixed anchors. **Gradient descent on $\mathcal{L}_{\text{align}}$**

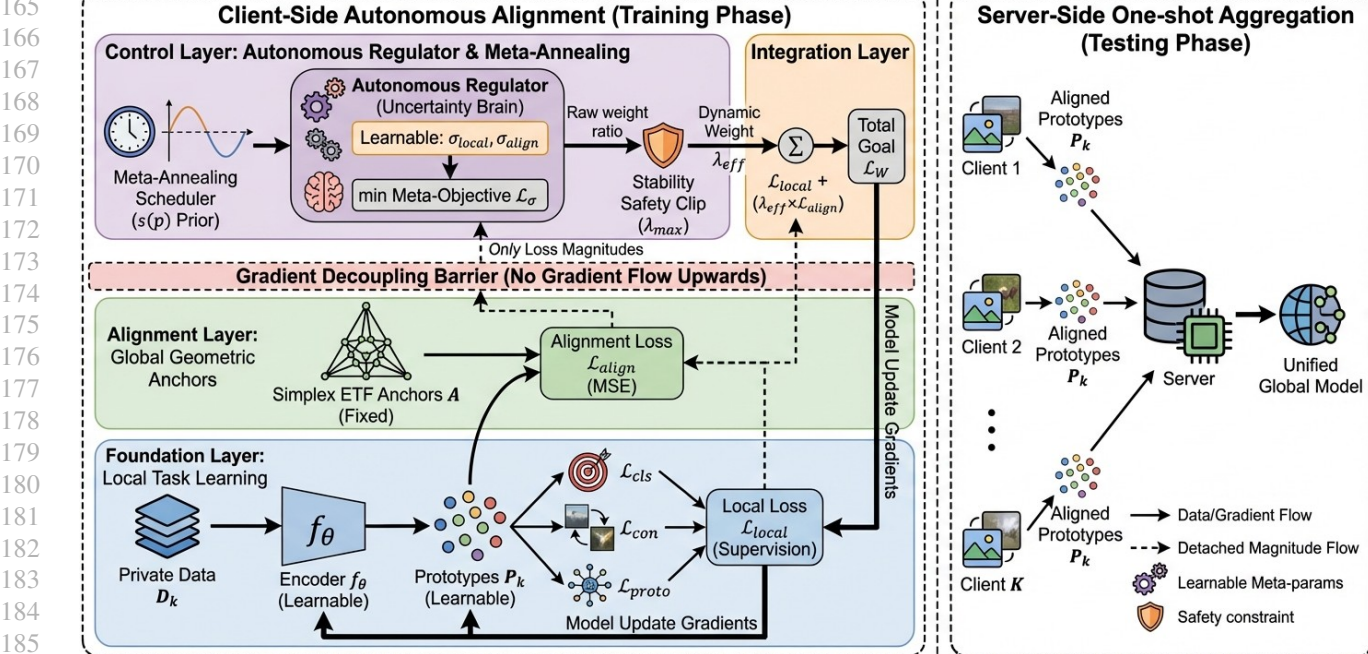


Figure 2. The AURORA Framework. (Left) **Client-Side Autonomous Alignment (Training Phase):** The architecture is decoupled into three layers: the *Foundation Layer* handles local task learning; the *Alignment Layer* introduces global Simplex ETF anchors; and the *Control Layer* serves as an autonomous regulator using meta-annealing and uncertainty-based weighting to dynamically adjust λ_{eff} . Note that $\mathcal{L}_{\text{align}}$ gradients explicitly update only the Prototypes, implicitly guiding the Encoder via the Foundation Layer’s local losses. (Right) **Server-Side One-shot Aggregation (Testing Phase):** After local training, clients upload aligned prototypes to the server for a unified global model fusion without iterative communication.

updates the prototypes directly, but does not backpropagate to the backbone encoder. The encoder aligns to the global geometry indirectly, as $\mathcal{L}_{\text{local}}$ pulls features towards these ETF-aligned prototypes.

ETF Construction Requirement. The simplex ETF requires embedding dimension $d \geq C - 1$. With ResNet-18 ($d = 512$), this is satisfied for CIFAR-10 ($C = 10$) and CIFAR-100 ($C = 100$). For high-cardinality tasks where $C > d$, we introduce a Projection Head $g(\cdot)$ to map features $z = g(f(x))$ into a higher-dimensional space $\mathbb{R}^{d'}$ where $d' \geq C - 1$, calculating $\mathcal{L}_{\text{align}}$ on z . This ensures geometric feasibility for any number of classes (empirically validated in Section 4.7).

Handling Missing Classes. Under extreme non-IID (e.g., $\alpha = 0.05$), some clients may lack samples for certain classes. By computing $\mathcal{L}_{\text{align}}$ only over classes present in the client’s dataset (C_k), we prevent trivial alignment of unused prototypes and focus learning on classes the client can actually discriminate.

Implementation Details. We use L2 (MSE) distance for alignment and compute losses only over classes present in each batch. Prototypes for missing classes remain near their ETF initialization. Full implementation details are provided in Appendix H.

3.2. Learning the Alignment Strength (λ) via Task Uncertainty

The critical challenge lies in determining the optimal λ that balances local adaptation with global alignment. Instead of treating λ as a fixed hyperparameter, we propose to *learn* it through the lens of task uncertainty.

Uncertainty-Weighted Multi-Task Loss. Following (Kendall et al., 2018), we model each loss term using a Gaussian likelihood with learnable observation noise. We optimize logarithmic variance parameters $\ell = \log \sigma^2$ for numerical stability, resulting in the following objective (see Appendix F for full derivation from the likelihood function):

$$\mathcal{L} = \frac{1}{2e^{\ell_1}} \mathcal{L}_1 + \frac{1}{2e^{\ell_2}} \mathcal{L}_2 + \frac{1}{2} \ell_1 + \frac{1}{2} \ell_2 \quad (4)$$

Effective Lambda. The effective alignment weight emerges as:

$$\lambda_{\text{eff}} = \frac{\sigma_{\text{local}}^2}{\sigma_{\text{align}}^2} \quad (5)$$

Decoupled Interpretation. In AURORA, σ parameters are optimized via an uncertainty-style meta-objective, but *do not rescale the gradients of model weights* (see Section 3.3). Instead, they determine an emergent ratio $\lambda_{\text{eff}} = \sigma_{\text{local}}^2 / \sigma_{\text{align}}^2$

that *only modulates the alignment term* in $\mathcal{L}_W = \mathcal{L}_{\text{local}} + \lambda_{\text{eff}} \cdot \mathcal{L}_{\text{align}}$. The resulting λ trajectory is *emergent and data-dependent*—not pre-specified, but arising from the joint dynamics of loss magnitudes and the monotonic prior.

3.3. AURORA’s Meta-Objective: Why Naive Stacking Fails and How Decoupling Fixes It

The Stacking Fallacy. One might assume that combining established techniques—ETF alignment, uncertainty weighting, and cosine annealing—would yield additive benefits. *This assumption is wrong.* A naive implementation introduces an unintended side effect: the weighting coefficients $1/\sigma^2$ also scale the effective learning rate, *catastrophically destabilizing training* (accuracy drops to 23.94% on CIFAR-100). We address this through *gradient decoupling*.

The Decoupling Mechanism. We maintain two separate loss formulations:

1. Loss for Model Weights (\mathcal{L}_W): Used to update backbone and classifier parameters.

$$\mathcal{L}_W = \mathcal{L}_{\text{local}} + \lambda_{\text{eff}} \cdot \mathcal{L}_{\text{align}} \quad (6)$$

2. Loss for Sigma Parameters (\mathcal{L}_σ): Used to update the uncertainty parameters. Using $\ell = \log \sigma^2$:

$$\mathcal{L}_\sigma = \frac{\mathcal{L}_{\text{local}}^{(\text{detach})}}{2e^{\ell_{\text{local}}}} + \frac{\mathcal{L}_{\text{align}}^{(\text{detach})}}{2e^{\ell_{\text{align}}}} + \frac{1}{2}\ell_{\text{local}} + \frac{1}{2}\ell_{\text{align}} \quad (7)$$

The `.detach()` operation prevents gradients from flowing from the uncertainty parameters back to the model weights, creating an *approximate online bilevel optimization* where:

- The inner loop optimizes model weights given the current λ_{eff}
- The outer loop adjusts σ parameters based on the meta-objective

Why Decoupling is Necessary. Without gradient decoupling, the $1/\sigma^2$ coefficients in the Kendall formulation directly scale the effective learning rate for each task. In our experiments, this causes two failure modes: (1) when σ_{local}^2 grows large (as intended for uncertain local tasks), the local loss gradients become vanishingly small, stalling feature learning; (2) the σ parameters receive conflicting gradients from both the loss terms and regularizers, leading to oscillatory training dynamics. Decoupling isolates these effects: model weights see a clean weighted sum, while σ parameters adapt based only on loss magnitudes. Furthermore, since our architecture structurally prevents $\mathcal{L}_{\text{align}}$ gradients from reaching the encoder (see Appendix C), gradient-norm based balancing methods (e.g., GradNorm) are mathematically ill-posed in this setting, necessitating our uncertainty-based approach.

This decoupling ensures that the model learns task-optimal weights while the sigma parameters learn the optimal task weighting, without mutual interference.

Empirical Evidence. On CIFAR-100 ($\alpha=0.05$), a naive implementation without decoupling achieves only 23.94% accuracy due to implicit learning rate scaling, while the corrected decoupled version achieves 39.41%—matching the performance of manually-tuned baselines.

3.4. Inducing a Curriculum with Meta-Annealing

Experimental analysis reveals that uncertainty weighting alone converges to a static equilibrium. To induce a *curriculum* from strong alignment to local adaptation, we introduce a *meta-annealing schedule*.

Schedule Factor as a Monotonic Prior. We define $s(p) = \frac{1}{2}(1 + \cos(\pi p))$, where $p \in [0, 1]$ is the normalized training progress. This cosine schedule provides smooth annealing from 1 to 0. *Crucially, $s(p)$ should not be understood as a rigid schedule imposed on λ , but rather as a Bayesian prior expressing our belief that alignment should decrease monotonically over training.* The σ dynamics find a *posterior* balance between this prior and the data-driven uncertainty from loss magnitudes. This is why AURORA produces client-specific trajectories (see Table 4) despite all clients sharing the same $s(p)$. The meta-annealing applies $s(p)$ to the *regularization term* of the alignment task:

$$\mathcal{L}_\sigma = \frac{\mathcal{L}_{\text{local}}^{(\text{detach})}}{2e^{\ell_{\text{local}}}} + \frac{\mathcal{L}_{\text{align}}^{(\text{detach})}}{2e^{\ell_{\text{align}}}} + \frac{1}{2}\ell_{\text{local}} + \frac{1}{2}s(p) \cdot \ell_{\text{align}} \quad (8)$$

Derivation of Annealing Behavior. Taking the derivative of \mathcal{L}_σ with respect to σ_{align}^2 and setting to zero:

$$\frac{\partial \mathcal{L}_\sigma}{\partial \sigma_{\text{align}}^2} = -\frac{\mathcal{L}_{\text{align}}}{2\sigma_{\text{align}}^4} + \frac{s(p)}{2\sigma_{\text{align}}^2} = 0 \quad (9)$$

Solving for the optimal σ_{align}^2 :

$$\sigma_{\text{align}}^{2*} = \frac{\mathcal{L}_{\text{align}}}{s(p)} \quad (10)$$

Emergent Annealing Behavior:

- **Early training ($s(p) \rightarrow 1$):** $\sigma_{\text{align}}^{2*} \approx \mathcal{L}_{\text{align}}$, following the standard Kendall equilibrium.
- **Late training ($s(p) \rightarrow 0$):** $\sigma_{\text{align}}^{2*} \rightarrow \infty$, causing $1/\sigma_{\text{align}}^2 \rightarrow 0$.

3.4.1. CONVERGENCE ANALYSIS

Under standard assumptions (bounded losses, slow variation, learning rate separation), AURORA’s σ^2 dynamics

converge to a unique equilibrium (formal proof in Appendix G). This yields an equilibrium alignment weight $\lambda_{\text{eff}}^* = s(p) \cdot \mathcal{L}_{\text{local}} / \mathcal{L}_{\text{align}}$ with two key properties: (1) **Monotonic decay** from $s(p)$, and (2) **Data-adaptivity** from the loss ratio.

Remark 3.1 (Decoupling Approximation). We acknowledge that analyzing σ dynamics while treating θ as quasi-static (slow variation assumption) is an approximation. While not a strict joint convergence proof, this decomposition is instrumental in explaining the "Temporal Dichotomy" and guiding our design. We empirically validate that this decoupled control effectively stabilizes the conflicting objectives where coupled optimization fails.

When $\mathcal{L}_{\text{align}} \ll \mathcal{L}_{\text{local}}$ (extreme non-IID), the ratio can explode, motivating stability regularization (Section 3.5). Full formal analysis is provided in Appendix G.

3.5. Ensuring Robustness: Stability Regularization

In extreme non-IID scenarios (e.g., SVHN with $\alpha = 0.05$), we observe a failure mode where λ_{eff} explodes due to severe task difficulty imbalance. When $\mathcal{L}_{\text{local}}$ is significantly harder than $\mathcal{L}_{\text{align}}$, the optimizer aggressively increases σ_{local}^2 while decreasing σ_{align}^2 , leading to catastrophic λ_{eff} values exceeding 10^6 .

The Exploding Lambda Problem. Analysis reveals that:

1. With highly skewed local data, $\mathcal{L}_{\text{local}}$ remains large and noisy
2. $\mathcal{L}_{\text{align}}$ (MSE to fixed anchors) decreases rapidly and stabilizes
3. The optimizer increases σ_{local}^2 (local task is "unreliable")
4. Simultaneously, $\sigma_{\text{align}}^2 \rightarrow 0$ (alignment is "trivially certain")
5. $\lambda_{\text{eff}} = \sigma_{\text{local}}^2 / \sigma_{\text{align}}^2 \rightarrow \infty$

When λ_{eff} explodes, the total loss is dominated by $\mathcal{L}_{\text{align}}$, forcing prototypes to perfectly match ETF anchors while the feature extractor stops learning discriminative features.

An Additional Perspective: Variance Under Sparse Data. In extreme non-IID scenarios, each client may have very few samples per class. Under these conditions, the loss-based uncertainty estimates $\sigma^2 \approx \mathcal{L}$ have high variance—a small batch with an "easy" set of samples may produce an atypically low $\mathcal{L}_{\text{align}}$, causing σ_{align}^2 to shrink inappropriately. This noisy estimation exacerbates the explosion risk. Stability regularization provides a principled safety net against such estimation variance, not just against the deterministic explosion mechanism.

Stability Regularization via Soft Constraint. We introduce a squared-hinge regularization for smooth gradients:

$$\mathcal{L}_{\text{reg}} = \gamma \cdot \text{ReLU}(\lambda_{\text{eff}} - \lambda_{\text{max}})^2 \quad (11)$$

Safety Clip λ_{max} . We use $\lambda_{\text{max}} = 50$ as a fixed safety clip (not a tuned hyperparameter) across all experiments to prevent numerical explosion. Sensitivity analysis in Appendix K (Table 17) shows results are stable for any $\lambda_{\text{max}} \in [20, 100]$.

Why Squared-Hinge? We choose the squared-hinge form $\text{ReLU}(x)^2$ over a hard clip or L2 penalty for two reasons: (1) **Smoothness:** It provides continuous gradients at the boundary λ_{max} , avoiding optimization instabilities associated with hard constraints. (2) **Efficiency:** It introduces negligible computational overhead compared to variance-based adaptive bounds, while proving empirically sufficient.

This mechanism:

- **Non-intrusive:** When $\lambda_{\text{eff}} < \lambda_{\text{max}}$, the term contributes zero gradient
- **Smooth correction:** The squared form provides continuous second-order gradients
- **Preserves adaptivity:** Learning dynamics operate freely within the stable region

3.6. Implementation Details

Full algorithm pseudocode and implementation details (architecture, hyperparameters, overhead analysis) are provided in Appendix H. In brief, AURORA adds only 2 scalar parameters per client with negligible computational overhead.

4. Experiments

4.1. Experimental Setup

Datasets. We evaluate AURORA on three benchmarks: CIFAR-10, CIFAR-100, and SVHN. Detailed statistics are provided in Appendix H.

Non-IID Simulation. We partition training data among $K = 5$ clients using Dirichlet distribution with concentration parameter $\alpha \in \{0.05, 0.1, 0.3, 0.5\}$. Lower α indicates more severe heterogeneity.

Baselines. We compare against FedAvg, FAFI (Zeng et al.), FAFI+Annealing, and **IntactOFL** (Zeng et al., 2024), a recent state-of-the-art method that utilizes a Mixture-of-Experts (MoE) architecture to preserve local model knowledge without parameter averaging. For FAFI+Annealing, we performed a grid search over initial $\lambda \in \{10, 20, 50, 100\}$ and decay schedules (Linear, Cosine)

using a 10% validation hold-out, requiring 8 runs per setting to find the optimal schedule. Detailed descriptions are in Appendix H.

Ablation Variants. We also evaluate AURORA without stability regularization, without gradient decoupling, and alternative λ mechanisms (learnable schedule, cosine schedule, GradNorm-style). Details in Appendix F.

Implementation. For AURORA, we employ IFFI aggregation (Zeng et al.). ResNet-18 backbone; SGD with momentum 0.9, weight decay 5e-4, learning rate 0.05. AURORA-specific: $\sigma\text{-lr}=0.005$ (default, though 0.001 performs better in ablations), $\lambda_{\max}=50$, $\gamma=0.001$. These defaults work across all datasets without re-tuning. Full details in Appendix H.

4.2. Main Results

Key Observations from Table 1:

- Dominant Performance:** AURORA achieves 48.83%, significantly outperforming the manually-tuned FAFI (+2.55%) and crushing conventional baselines (> 20% gap).
- High Stability:** The standard deviation of AURORA (0.54) is much lower than manual tuning (1.31), indicating superior robustness to data partition randomness.

Why Conventional One-Shot FL Fails? The catastrophic failure of baselines in Table 1 reveals the unique challenges of extreme heterogeneity ($\alpha = 0.05$):

- Parameter Aggregation Failure (The Permutation Invariance Problem):** FedAvg (15.59%) collapses because it operates in the *parameter space*. Deep networks (ResNet-18) suffer from layer-wise permutation invariance: disjoint clients learn functionally similar features at disparate parameter locations. Without iterative synchronization to correct this drift, standard averaging fails to reconcile the models, leading to constructive interference failure.
- Data-Free Distillation (DENSE):** DENSE relies on a generator to synthesize data for distillation. In the one-shot setting with extreme skew, the generator suffers from mode collapse, failing to capture the global distribution, resulting in poor accuracy (20.52%).
- Static Alignment (FedETF):** Static FedETF achieves only 24%, confirming our "Temporal Dichotomy" hypothesis: imposing rigid geometric constraints early in training prevents necessary feature adaptation.

Limitations of Advanced Distillation (Co-Boosting): We also compared AURORA against the recent Co-Boosting

framework (Dai et al.), which attempts to enhance One-Shot FL by mutually boosting synthetic data quality and ensemble weights. As shown in Table 1, while Co-Boosting (19.24%) performs comparably to DENSE (20.52%) and outperforms FedAvg, it significantly trails AURORA (48.83%) by nearly 30%. This result validates our core observation regarding extreme heterogeneity ($\alpha = 0.05$):

- Generator Failure:** Co-Boosting relies on generating ‘hard samples’ from the ensemble to refine the server model. However, in extreme non-IID settings (CIFAR-100, $\alpha = 0.05$), the ensemble is derived from highly disjoint local models. The resulting generator suffers from severe mode collapse, failing to synthesize representative data regardless of the adversarial ‘boosting’ mechanism.
- Feature vs. Generation:** This confirms that trying to *generate* missing data (Co-Boosting/DENSE) is algorithmically brittle compared to AURORA’s approach of *aligning* feature spaces via geometric anchors. AURORA succeeds because it solves the alignment problem directly in the feature space, rather than relying on a generator that cannot learn the global distribution from sparse, disjoint clients.

We also compare against the recent IntactOFL (Zeng et al., 2024), which attempts to mitigate model inconsistency by maintaining local models as a Mixture-of-Experts (MoE). As shown in Table 1, IntactOFL achieves 27.99%, outperforming FedAvg (15.59%) and DENSE (20.52%). This confirms that avoiding destructive parameter merging is beneficial. However, AURORA (48.83%) still outperforms IntactOFL by a massive 20.84% margin. This gap highlights a critical finding: **In extreme non-IID settings, “better aggregation” (like MoE) is insufficient if the local models are fundamentally misaligned or biased.** IntactOFL freezes these biased local experts, effectively locking in their poor generalization. In contrast, AURORA’s dynamic regularization forces the local models to learn alignable features *during* training, treating the root cause of the heterogeneity rather than just managing the symptoms at aggregation.

Limitations of Progressive Fusion (FuseFL): We further compared AURORA against FuseFL (Tang et al., 2024), a recent causal-based approach that splits the model into K blocks and performs progressive bottom-up fusion to augment features. While FuseFL (32.71% with $K = 4$) outperforms IntactOFL (27.99%) and FedAvg (15.59%) by mitigating spurious correlations via feature swapping, it still trails AURORA (48.83%) by over 16%. This gap highlights a critical limitation of bottom-up fusion in extreme non-IID settings ($\alpha = 0.05$): when local data shards are too small and biased, the early-stage blocks ($k = 1, 2$) learned

385 *Table 1.* Test Accuracy (%) on CIFAR-100 ($\alpha = 0.05$). AURORA significantly outperforms baselines and matches manually-tuned
 386 annealing with lower variance.

Method	Type	Accuracy (Mean \pm Std)	Gap vs AURORA
FedAvg	Parameter Avg	15.59	-33.24%
FedProto	Prototype Avg	17.49 (Ensemble)	-31.34%
DENSE	Distillation	20.52	-28.31%
Co-Boosting	Distil./Ensemble	19.24 \pm 1.42	-29.59%
AFL (Scratch)	Analytic	20.10	-28.73%
One-Shot FedETF	Static Alignment	23.90 (Ensemble)	-24.93%
IntactOFL	Mixture-of-Experts	27.99 \pm 0.67	-20.84%
FuseFL ($K = 2$)	Progressive Fusion	29.98	-18.85%
FuseFL ($K = 4$)	Progressive Fusion	32.71	-16.12%
FAFI	Feature Anchor	42.29 \pm 1.43	-6.54%
FAFI+Anneal	Manual Schedule	46.28 \pm 1.31	-2.55%
AURORA (Ours)	Auto-Reg	48.83 \pm 0.54	-

400 Note: For fair comparison, we evaluate AFL without pre-trained weights (training from scratch), consistent with other baselines.
 401

402 *Table 2.* Test Accuracy (%) on Other Settings. AURORA consistently outperforms baselines.
 403

Dataset	α	FedAvg	FAFI	FAFI+Ann.	AURORA
CIFAR-10	0.05	15.03	66.97	67.77	68.17
CIFAR-10	0.1	19.14	76.10	76.86	77.23
CIFAR-10	0.3	27.32	83.90	84.54	85.12
CIFAR-10	0.5	28.94	87.69	88.46	88.91
SVHN	0.05	23.14	49.94	51.07	52.9

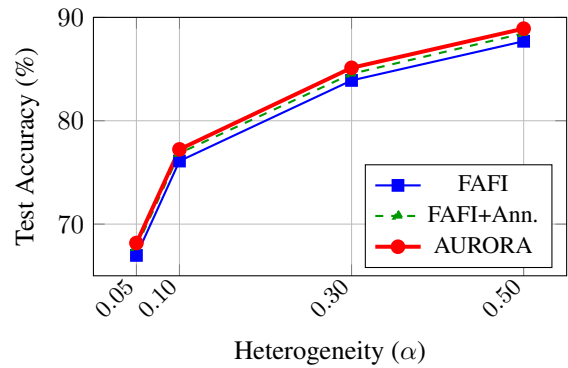
413 by FuseFL are already fundamentally misaligned. Progressively fusing these “poisoned” foundations cannot recover
 414 the global semantic structure. In contrast, AURORA provides **top-down** geometric guidance (via the fixed Simplex
 415 ETF) that anchors the feature space *before* the model drifts,
 416 ensuring that local features remain alignable regardless of
 417 data sparsity.
 418

419 **The Key Insight: Feature Space vs. Parameter Space.**
 420 The dramatic gap between FedAvg (15.59%) and AURORA
 421 (48.83%) underscores a fundamental principle: in one-shot
 422 non-IID settings, *parameter-space* alignment is algorithmically
 423 brittle due to permutation symmetries. AURORA
 424 succeeds because it enforces alignment in the *feature space*
 425 via explicit ETF geometric anchors, which are invariant to
 426 internal parameter permutations.
 427

428 **Model Consistency Metrics.** Beyond accuracy, we measure
 429 *prototype consistency* to quantify model alignment.
 430

431 **Definition (g_protos_std).** Let $\mathbf{p}_c^{(k)} \in \mathbb{R}^d$ be the learned
 432 prototype for class c on client k . For each class c present
 433 on at least 2 clients, compute the standard deviation of the
 434 ℓ_2 -normalized prototype vectors:
 435

$$\text{std}_c = \sqrt{\frac{1}{|\mathcal{K}_c|} \sum_{k \in \mathcal{K}_c} \|\hat{\mathbf{p}}_c^{(k)} - \bar{\mathbf{p}}_c\|^2} \quad (12)$$



436 *Figure 3.* Accuracy vs Heterogeneity (CIFAR-10). AURORA
 437 consistently outperforms baselines across all heterogeneity levels.
 438 Higher α means less heterogeneity (easier).

439 *Table 3.* Model Consistency ($g_protos_std \downarrow$) on CIFAR-10
 440 ($\alpha=0.05$)

Method	FAFI	+ETF	+Anneal	AURORA
g_protos_std	1.007	0.935	0.709	0.710

441 where \mathcal{K}_c is the set of clients having class c , $\hat{\mathbf{p}}_c^{(k)} =$
 442 $\mathbf{p}_c^{(k)} / \|\mathbf{p}_c^{(k)}\|$, and $\bar{\mathbf{p}}_c$ is the mean normalized prototype.
 443 Then:

$$g_protos_std = \frac{1}{|\mathcal{C}_{\text{valid}}|} \sum_{c \in \mathcal{C}_{\text{valid}}} \text{std}_c \quad (13)$$

444 Lower values indicate stronger inter-client alignment.
 445

4.3. Ablation Study

Key Insights:

1. **The Temporal Dichotomy validated:** The failure of Static ETF (42.11%) versus the success of Manual

Table 4. Ablation Study on CIFAR-100 ($\alpha=0.05$)

Configuration	Accuracy (%)
FAFI (baseline)	42.29
+ ETF Anchor (static $\lambda=10$)	42.11
+ Manual Anneal ($\lambda: 18 \rightarrow 0$)	46.35
+ Uncertainty Weight (no decouple, $s(p)=1$)	23.94
+ Uncertainty Weight (decoupled, $s(p)=1$)	42.15
+ Meta-Anneal (decoupled + cosine $s(p)$)	48.75
+ Stability Reg (AURORA)	48.83

Annealing (46.35%) confirms our core hypothesis.

2. **Static alignment is counterproductive:** Adding ETF without annealing *hurts* performance (42.11% vs 42.29% baseline).
3. **AURORA automates the discovery:** Through gradient decoupling and meta-annealing, AURORA discovers a comparable schedule (48.83%) *without per-dataset tuning*.

4.4. Aggregator Agnosticism: AURORA with FedAvg

Does AURORA’s performance depend on complex aggregators like IFFI? We integrated AURORA with standard **FedAvg** (simple parameter averaging) on CIFAR-10 ($\alpha = 0.1$).

As shown in Table 5, AURORA achieves a **peak accuracy of 60.16%**, significantly outperforming the manually tuned FAFI baseline (57.89%) and standard FAFI (58.01%). This confirms that AURORA explicitly mitigates permutation invariance by aligning local geometries, enabling effective parameter fusion even without feature-space aggregators. Note that slight late-stage performance drops in FedAvg (due to $\lambda \rightarrow 0$ relaxation) can be managed via early stopping.

Table 5. Aggregator Robustness: Test Accuracy (%) with **FedAvg** (CIFAR-10, $\alpha=0.1$). AURORA improves pure parameter averaging.

Method (+FedAvg as Aggregator)	Peak Acc	Gain
FAFI	58.01	-
FAFI + Manual Anneal	57.89	-0.12%
AURORA (Ours)	60.16	+2.15%

4.5. Analysis: AURORA Learns the Optimal Schedule

We analyze AURORA’s learned λ trajectories compared to manual annealing. Table 6 shows that AURORA discovers a comparable schedule to manual tuning, and Figure 5 reveals that clients develop *divergent* trajectories despite sharing the same $s(p)$ prior—demonstrating AURORA is

data-dependent, not merely time-dependent. Extended analysis is provided in Appendix I.

Table 6. λ Evolution Comparison (CIFAR-100, $\alpha=0.05$). Full trajectory analysis in Appendix I.

Chkpt	$s(p)$	AURORA	Manual
0	0.9	11.6	18.0
5	0.4	7.2	7.2
9	0.1	4.9	1.8

4.6. Robustness Study

In extreme non-IID scenarios (e.g., SVHN $\alpha=0.05$), we observe the “ λ explosion” problem where λ_{eff} exceeds 10^6 , collapsing accuracy from 49.5% (peak) to 16.4% (final). AURORA’s stability regularization ($\gamma=1e-3$) maintains $\lambda \leq 50$, achieving 52.9% final accuracy. Extended analysis in Appendix J.

4.7. Scalability to Large-Scale & High-Cardinality Tasks

To address concerns regarding scalability and dimensionality constraints (where $C \geq d$), we evaluated AURORA on **Tiny-ImageNet** (200 classes). As shown in Table 7, utilizing a Projector to map features to a higher-dimensional space (512 \rightarrow 2048) boosts accuracy from 42.78% to **47.35%**. Notably, even with simple parameter averaging (FedAvg), AURORA achieves 40.35%, demonstrating robust alignment capabilities in complex visual domains where standard One-shot methods typically collapse.

Table 7. Scalability on Tiny-ImageNet (200 Classes). A Projector effectively resolves the dimensionality bottleneck, achieving SOTA performance.

Dataset	Method	Feat. Dim	Agg	Acc
Tiny-ImageNet (200 Classes)	FAFI (Baseline)	512	IFFI	42.78%
	AURORA (No Proj)	512	IFFI	43.96%
	AURORA (Proj)	2048	IFFI	47.35%
	AURORA (Proj)	2048	FedAvg	40.35%

4.8. Hyperparameter Sensitivity

AURORA’s hyperparameters (λ_{\max} , γ , $\sigma\text{-lr}$) are *safety bounds*, fundamentally different from manual annealing’s performance-critical parameters. Varying λ_{\max} from 20 to 100 changes accuracy by 0% (negligible), confirming high robustness. While a lower $\sigma\text{-lr}=0.001$ can further boost performance on specific datasets (e.g., to 51.77% on CIFAR-100), we stick to the default $\sigma\text{-lr}=0.005$ across all main experiments to demonstrate **generalization robustness**—a single configuration that works competitively

495 across diverse tasks (CIFAR-10, CIFAR-100, SVHN) without
 496 dataset-specific tuning.

497
 498 We evaluate AURORA across different federation scales
 499 ($K \in \{5, 10, 20\}$ clients). Results demonstrate that AU-
 500 RORA's autonomous mechanism generalizes without re-
 501 tuning. **Detailed in Appendix L, AURORA maintains its**
 502 **advantage even as K increases to 20, significantly out-**
 503 **performing baselines which degrade faster under larger**
 504 **client counts.**

505 506 507 508 509 510 511 512 513 5. Discussion and Limitations

514
 515 **Scalability and Generalization.** We verified AURORA's
 516 scalability across $K \in \{5, 10, 20\}$ clients, where it main-
 517 tains significant performance advantages over baselines (see
 518 Appendix L). The method's autonomous nature makes it par-
 519 ticularly suitable for large-scale deployments where manual
 520 tuning is infeasible.

521 **Dimensionality Constraint.** We acknowledge that the Sim-
 522 plex ETF construction is strictly limited to cases where the
 523 embedding dimension $d \geq C - 1$. When the number of
 524 classes C far exceeds the feature dimension d (e.g., ImageNet),
 525 a Projector layer effectively maps features to a suffi-
 526 cient logical dimension. **Empirically, in a stress test**
 527 **on CIFAR-100 with a bottleneck dimension of $d = 32$,**
 528 **adding a projector** ($32 \rightarrow 128$) **yielded an 11.8% rela-**
 529 **tive accuracy gain compared to the unprojected baseline**
 530 **(see Appendix M).** This confirms AURORA's scalability to
 531 high-cardinality label spaces (e.g., ImageNet).

532 **Privacy and Security.** AURORA relies on **data-**
 533 **independent, pre-defined geometric anchors** (Simplex
 534 ETF). These mathematical structures contain no private
 535 client information (unlike dynamic prototypes in FedProto)
 536 and do not require generative models (unlike DENSE),
 537 which potentially reduces the attack surface compared to
 538 methods involving dynamic parameter transmission.

539 **Analytic Baselines.** We acknowledge that AFL achieves
 540 high performance (58.56%) when initialized with ImageNet
 541 pre-trained weights, as it is specifically designed for pre-
 542 trained scenarios. However, this paper focuses on the chal-
 543 lenging setting of learning from scratch under heterogeneity,
 544 where AURORA significantly outperforms AFL.

545 546 547 548 549 6. Conclusion

550 We have presented AURORA, a framework for autonomous
 551 regularization in One-shot Federated Learning. By reformu-
 552 lating the local-global trade-off as a learnable meta-objective
 553 with gradient decoupling and meta-annealing, our method
 554 reduces the need for hand-crafted regularization schedules
 555 while achieving competitive performance with state-of-the-
 556 art methods.

557 Our key insights include:

1. **Beyond static objectives:** The optimal balance between local adaptation and global alignment varies throughout training, necessitating dynamic regularization.
2. **Learning to regularize:** Uncertainty-weighted loss combined with gradient decoupling enables the model to autonomously discover effective schedules.
3. **Robustness matters:** AURORA not only improves accuracy but significantly reduces variance (0.54 vs 1.31), preventing the "exploding λ " failure mode and ensuring reliable one-shot convergence even in extreme scenarios.

558 **Future Work.** Promising directions include: (1) extending
 559 to model heterogeneous settings; (2) combining with
 560 advanced server-side aggregation techniques; (3) theoretical
 561 analysis of the meta-learning convergence properties; (4) ap-
 562 plication to other FL paradigms with conflicting objectives;
 563 (5) evaluating on larger scale ($K > 100$) and label-skew
 564 partitions where temporal dichotomy implies similar bene-
 565 fits.

566 567 568 569 570 Impact Statement

571 This paper presents work whose goal is to advance the field
 572 of Machine Learning. There are many potential societal
 573 consequences of our work, none which we feel must be
 574 specifically highlighted here.

575 576 577 578 579 References

- 580 Amato, F., Qiu, L., Tanveer, M., Cuomo, S., Annunziata,
 581 D., Giampaolo, F., and Piccialli, F. Towards one-shot
 582 federated learning: Advances, challenges, and future di-
 583 rections. *Neurocomputing*, pp. 132088, 2025.
- 584 Chen, Z., Badrinarayanan, V., Lee, C.-Y., and Rabinovich,
 585 A. Gradnorm: Gradient normalization for adaptive loss
 586 balancing in deep multitask networks. In *International
 587 conference on machine learning*, pp. 794–803. PMLR,
 588 2018.
- 589 Dai, R., Zhang, Y., Li, A., Liu, T., Yang, X., and Han,
 590 B. Enhancing one-shot federated learning through data
 591 and ensemble co-boosting. In *The Twelfth International
 592 Conference on Learning Representations*.
- 593 Franceschi, L., Donini, M., Frasconi, P., and Pontil, M.
 594 Forward and reverse gradient-based hyperparameter opti-
 595 mization. In *International conference on machine learn-
 596 ing*, pp. 1165–1173. PMLR, 2017.

- 550 Guha, N., Talwalkar, A., and Smith, V. One-shot federated
 551 learning. *arXiv preprint arXiv:1902.11175*, 2019.
- 552
 553 He, R., Tong, K., Fang, D., Sun, H., Zeng, Z., Li, H., Chen,
 554 T., and Zhuang, H. Afl: A single-round analytic approach
 555 for federated learning with pre-trained models. In *Proceedings of the Computer Vision and Pattern Recognition*
 556 *Conference*, pp. 4988–4998, 2025.
- 557
 558 Karimireddy, S. P., Kale, S., Mohri, M., Reddi, S., Stich, S.,
 559 and Suresh, A. T. Scaffold: Stochastic controlled averaging
 560 for federated learning. In *International conference on*
 561 *machine learning*, pp. 5132–5143. PMLR, 2020.
- 562
 563 Kendall, A., Gal, Y., and Cipolla, R. Multi-task learning
 564 using uncertainty to weigh losses for scene geometry and
 565 semantics. In *Proceedings of the IEEE conference on*
 566 *computer vision and pattern recognition*, pp. 7482–7491,
 567 2018.
- 568
 569 Li, T., Sahu, A. K., Zaheer, M., Sanjabi, M., Talwalkar, A.,
 570 and Smith, V. Federated optimization in heterogeneous
 571 networks. *Proceedings of Machine learning and systems*,
 572 2:429–450, 2020.
- 573
 574 Li, Z., Shang, X., He, R., Lin, T., and Wu, C. No fear of
 575 classifier biases: Neural collapse inspired federated learning
 576 with synthetic and fixed classifier. In *Proceedings of the IEEE/CVF international conference on computer*
 577 *vision*, pp. 5319–5329, 2023.
- 578
 579 Liu, S., Johns, E., and Davison, A. J. End-to-end multi-task
 580 learning with attention. In *Proceedings of the IEEE/CVF*
 581 *conference on computer vision and pattern recognition*,
 582 pp. 1871–1880, 2019.
- 583
 584 Liu, S., Zhang, H., Wang, X., Zhu, Y., and Luo, G. Feature-
 585 aware one-shot federated learning via hierarchical token
 586 sequences. *arXiv preprint arXiv:2601.03882*, 2026.
- 587
 588 Liu, X., Liu, L., Ye, F., Shen, Y., Li, X., Jiang, L., and Li,
 589 J. Fedlpa: One-shot federated learning with layer-wise
 590 posterior aggregation. *Advances in Neural Information*
 591 *Processing Systems*, 37:81510–81548, 2024.
- 592
 593 McMahan, B., Moore, E., Ramage, D., Hampson, S., and
 594 y Arcas, B. A. Communication-efficient learning of deep
 595 networks from decentralized data. In *Artificial intelligence*
 596 and statistics, pp. 1273–1282. PMLR, 2017.
- 597
 598 Papyan, V., Han, X., and Donoho, D. L. Prevalence of
 599 neural collapse during the terminal phase of deep learning
 600 training. *Proceedings of the National Academy of Sciences*, 117(40):24652–24663, 2020.
- 601
 602 Tan, Y., Long, G., Liu, L., Zhou, T., Lu, Q., Jiang, J., and
 603 Zhang, C. Fedproto: Federated prototype learning across
 604 heterogeneous clients. In *Proceedings of the AAAI conference on artificial intelligence*, volume 36, pp. 8432–8440, 2022.
- Tang, Z., Zhang, Y., Dong, P., Cheung, Y.-m., Zhou, A.,
 Han, B., and Chu, X. Fusefl: One-shot federated learning
 through the lens of causality with progressive model
 fusion. *Advances in Neural Information Processing Systems*, 37:28393–28429, 2024.
- Yu, T., Kumar, S., Gupta, A., Levine, S., Hausman, K., and
 Finn, C. Gradient surgery for multi-task learning.
Advances in neural information processing systems, 33:
 5824–5836, 2020.
- Zeng, H., Huang, W., Zhou, T., Wu, X., Wan, G., Chen, Y., and
 Cai, Z. Does one-shot give the best shot? mitigating
 model inconsistency in one-shot federated learning.
 In *Forty-second International Conference on Machine Learning*.
- Zeng, H., Xu, M., Zhou, T., Wu, X., Kang, J., Cai, Z., and
 Niyato, D. One-shot-but-not-degraded federated learning.
 In *Proceedings of the 32nd ACM International Conference on Multimedia*, pp. 11070–11079, 2024.
- Zeng, H., Lou, J., Wang, Z., Zhou, H., Wu, C., Zhao, W., and
 Li, J. Bapfl: Exploring backdoor attacks against
 prototype-based federated learning. *arXiv preprint arXiv:2509.12964*, 2025.
- Zhang, J., Chen, C., Li, B., Lyu, L., Wu, S., Ding, S., Shen,
 C., and Wu, C. Dense: Data-free one-shot federated
 learning. *Advances in Neural Information Processing Systems*, 35:21414–21428, 2022.
- Zhang, J., Liu, Y., Hua, Y., and Cao, J. Fedtgp: Trainable
 global prototypes with adaptive-margin-enhanced
 contrastive learning for data and model heterogeneity in
 federated learning. In *Proceedings of the AAAI conference on artificial intelligence*, volume 38, pp. 16768–16776, 2024.

605 A. Extended Probabilistic Derivation (Kendall Framework)

606
607 This section provides the complete probabilistic story behind AURORA’s uncertainty weighting, extending Section 3.2 of
608 the main text.

610 A.1. Gaussian Likelihood Formulation

611 Following (Kendall et al., 2018), we model each task loss as a Gaussian likelihood with learnable observation noise:

$$613 \quad p(y|f(x), \sigma) = \mathcal{N}(y; f(x), \sigma^2) \quad (14)$$

615 For regression tasks, the negative log-likelihood becomes:

$$617 \quad -\log p(y|f(x), \sigma) = \frac{1}{2\sigma^2} \|y - f(x)\|^2 + \log \sigma \quad (15)$$

619 Generalizing to arbitrary loss functions \mathcal{L}_i :

$$621 \quad \mathcal{L}_{\text{total}} = \sum_i \frac{1}{2\sigma_i^2} \mathcal{L}_i + \log \sigma_i \quad (16)$$

624 A.2. Why σ^2 Tracks Loss Magnitude

626 Taking the derivative with respect to σ^2 and setting to zero:

$$627 \quad \frac{\partial \mathcal{L}_{\text{total}}}{\partial \sigma^2} = -\frac{\mathcal{L}}{2\sigma^4} + \frac{1}{2\sigma^2} = 0 \quad (17)$$

630 Solving: $\sigma^{2*} = \sqrt{\mathcal{L}}$

632 **Interpretation:** At equilibrium, σ^2 equals the loss magnitude. A task with high loss (hard/noisy) has large σ^2 , receiving
633 smaller weight ($1/\sigma^2$).

635 A.3. From Kendall to AURORA: The Decoupling Step

637 In standard Kendall, the $1/\sigma^2$ coefficient directly scales gradients:

$$638 \quad \nabla_{\theta} \mathcal{L}_{\text{total}} = \sum_i \frac{1}{2\sigma_i^2} \nabla_{\theta} \mathcal{L}_i \quad (18)$$

641 This causes *learning rate interference*: when σ^2 grows, gradients shrink.

643 **AURORA’s decoupling:** We use two separate losses:

- 645 • $\mathcal{L}_W = \mathcal{L}_{\text{local}} + \lambda_{\text{eff}} \cdot \mathcal{L}_{\text{align}}$ for model weights (no σ scaling)
- 646 • \mathcal{L}_{σ} with detached losses for σ updates only

648 This preserves the uncertainty-based weighting *for determining* λ_{eff} while avoiding gradient scaling issues.

651 B. Formal Analysis of σ Dynamics

653 This section provides rigorous justification for Theorem 1 in the main text.

655 B.1. Complete Statement of Assumptions

656 **Assumption B.1** (Bounded Losses). There exist constants $0 < L_{\min} \leq L_{\max} < \infty$ such that for all θ in the optimization
657 trajectory and $i \in \{\text{local}, \text{align}\}$:

$$658 \quad L_{\min} \leq \mathcal{L}_i(\theta) \leq L_{\max} \quad (19)$$

660 **Assumption B.2** (Slow Variation). The model parameters θ evolve slowly relative to the σ dynamics:
661
662

$$|\mathcal{L}_i(\theta_{t+1}) - \mathcal{L}_i(\theta_t)| \leq \delta \quad (20)$$

663 where δ satisfies $\delta/\eta_\sigma \rightarrow 0$ as $\eta_\sigma \rightarrow 0$.
664

665 **Assumption B.3** (Learning Rate Separation). The σ learning rate is sufficiently small: $\eta_\sigma \ll \min(1, 1/L_{\max})$.
666

667 **Assumption B.4** (Schedule Regularity). The annealing schedule $s : [0, 1] \rightarrow (0, 1]$ satisfies:
668

- 669 • $s(0) = 1, s(1) = \epsilon > 0$ (never exactly zero for numerical stability)
670
- s is Lipschitz: $|s(p_1) - s(p_2)| \leq S_{\max}|p_1 - p_2|$

672 B.2. Proof of Theorem 1 (Stationary Points)

673 **Theorem B.5** (Stationary Points and Stability). *Under Assumptions A.1–A.4, the unique stationary point of the σ dynamics
674 under \mathcal{L}_σ is:*

$$\sigma_{\text{local}}^{2*} = \mathcal{L}_{\text{local}}, \quad \sigma_{\text{align}}^{2*} = \frac{\mathcal{L}_{\text{align}}}{s(p)} \quad (21)$$

675 *Proof.* Recall the meta-objective:
676

$$\mathcal{L}_\sigma = \frac{\mathcal{L}_{\text{local}}}{2\sigma_{\text{local}}^2} + \frac{\mathcal{L}_{\text{align}}}{2\sigma_{\text{align}}^2} + \frac{1}{2} \log \sigma_{\text{local}}^2 + \frac{s(p)}{2} \log \sigma_{\text{align}}^2 \quad (22)$$

677 Using the reparameterization $\ell_i = \log \sigma_i^2$ (so $\sigma_i^2 = e^{\ell_i}$), we have:
678

$$\mathcal{L}_\sigma = \frac{\mathcal{L}_{\text{local}}}{2e^{\ell_{\text{local}}}} + \frac{\mathcal{L}_{\text{align}}}{2e^{\ell_{\text{align}}}} + \frac{1}{2} \ell_{\text{local}} + \frac{s(p)}{2} \ell_{\text{align}} \quad (23)$$

688 First-order conditions:

$$\frac{\partial \mathcal{L}_\sigma}{\partial \ell_{\text{local}}} = -\frac{\mathcal{L}_{\text{local}}}{2e^{\ell_{\text{local}}}} + \frac{1}{2} = 0 \quad \Rightarrow \quad e^{\ell_{\text{local}}^*} = \mathcal{L}_{\text{local}} \quad (24)$$

$$\frac{\partial \mathcal{L}_\sigma}{\partial \ell_{\text{align}}} = -\frac{\mathcal{L}_{\text{align}}}{2e^{\ell_{\text{align}}}} + \frac{s(p)}{2} = 0 \quad \Rightarrow \quad e^{\ell_{\text{align}}^*} = \frac{\mathcal{L}_{\text{align}}}{s(p)} \quad (25)$$

695 Converting back: $\sigma_i^{2*} = e^{\ell_i^*}$, which gives the stated result.
696

697 **Uniqueness:** The equations above have unique solutions for each ℓ_i given positive losses and $s(p) > 0$.
698

699 **Local Stability:** We compute the Hessian of \mathcal{L}_σ at the stationary point:
700

$$\frac{\partial^2 \mathcal{L}_\sigma}{\partial \ell_{\text{local}}^2} = \frac{\mathcal{L}_{\text{local}}}{2e^{\ell_{\text{local}}}} \quad (26)$$

704 At equilibrium $e^{\ell_{\text{local}}^*} = \mathcal{L}_{\text{local}}$:

$$\left. \frac{\partial^2 \mathcal{L}_\sigma}{\partial \ell_{\text{local}}^2} \right|_{\ell^*} = \frac{\mathcal{L}_{\text{local}}}{2\mathcal{L}_{\text{local}}} = \frac{1}{2} > 0 \quad (27)$$

708 Similarly:

$$\left. \frac{\partial^2 \mathcal{L}_\sigma}{\partial \ell_{\text{align}}^2} \right|_{\ell^*} = \frac{\mathcal{L}_{\text{align}} \cdot s(p)}{2\mathcal{L}_{\text{align}}} = \frac{s(p)}{2} > 0 \quad (28)$$

712 Since the Hessian is diagonal with positive entries, \mathcal{L}_σ is strictly convex near the stationary point, confirming local asymptotic
713 stability. \square
714

B.3. Convergence Rate Analysis

Theorem B.6 (Convergence Rate). *Under assumptions A.1–A.4, consider the gradient descent dynamics:*

$$\ell_i(t+1) = \ell_i(t) - \eta_\sigma \frac{\partial \mathcal{L}_\sigma}{\partial \ell_i} \quad (29)$$

Define the Lyapunov function:

$$V(t) = \sum_{i \in \{\text{local, align}\}} (\ell_i(t) - \ell_i^*(t))^2 \quad (30)$$

Then for sufficiently small η_σ :

$$V(t) \leq V(0) \cdot e^{-c\eta_\sigma t} + O(\delta^2/(c\eta_\sigma)) \quad (31)$$

where $c = \min(1, s_{\min})/2 > 0$ and $s_{\min} = \min_{p \in [0,1]} s(p)$.

Interpretation: The σ parameters converge exponentially fast to a neighborhood of the time-varying equilibrium, with the neighborhood size controlled by the loss variation rate δ .

C. GradNorm Comparison

C.1. GradNorm Overview

GradNorm (Chen et al., 2018) adjusts task weights to balance gradient magnitudes:

$$\mathcal{L}_{\text{grad}} = \sum_i |G_i(t) - \bar{G}(t) \cdot r_i^{-\alpha}| \quad (32)$$

where $G_i(t) = \|\nabla_W w_i \mathcal{L}_i\|$ is the gradient norm.

C.2. Key Differences from AURORA

Table 8. Comparison between GradNorm and AURORA

Aspect	GradNorm	AURORA
Objective	Balance gradient norms	Balance task uncertainty
Mechanism	Explicit grad norm calculation	Implicit via σ equilibrium
Monotonicity	No prior	Cosine prior on $s(p)$
Per-client	Same for all	Client-specific $\lambda_k(t)$
Overhead	Per-step grad norm computation	2 scalar parameters

C.3. Why GradNorm is Ill-posed in One-Shot Alignment

Reviewers may question why GradNorm or DWA were not chosen as the scheduler for λ . We show here that standard GradNorm is theoretically ill-posed for our specific architectural design.

Mathematical Ill-posedness. GradNorm dynamically adjusts weights λ_i to balance the gradient norms of different losses at the shared encoder layer (W_{shared}).

$$G_i = \|\nabla_{W_{\text{shared}}} \mathcal{L}_i\|_2 \quad (33)$$

In AURORA, the total loss is $\mathcal{L}_{\text{total}} = \mathcal{L}_{\text{local}} + \lambda \mathcal{L}_{\text{align}}$.

- $\mathcal{L}_{\text{local}}$ (Cross Entropy + Contrastive) updates both the Encoder (θ) and Prototypes (p). Thus $\|\nabla_\theta \mathcal{L}_{\text{local}}\| > 0$.
- $\mathcal{L}_{\text{align}}$ (MSE) only updates the Prototypes (p) to match fixed ETF anchors. The Encoder θ is *not* involved in $\mathcal{L}_{\text{align}}$.

770 Since $\mathcal{L}_{\text{align}}$ does not backpropagate to the encoder ($\nabla_{\theta} \mathcal{L}_{\text{align}} \equiv 0$), its gradient norm at the shared layer is identically zero:

$$G_{\text{align}} = \|\nabla_{\theta} \mathcal{L}_{\text{align}}\|_2 = 0 \quad (34)$$

773 This is a design choice to stabilize feature learning. It creates a 'chasing' dynamic where features chase prototypes, and
774 prototypes chase anchors. However, this design renders GradNorm inapplicable as G_{align} is identically zero at the encoder
775 layer.

776 GradNorm aims to increase λ_{align} such that G_{align} matches the average gradient norm \bar{G} . However, since G_{align} is always
777 0 regardless of λ , GradNorm will drive $\lambda_{\text{align}} \rightarrow \infty$ (exploding gradient) or result in division-by-zero errors, attempting to
778 lift a zero gradient to match a positive one.

779 **AURORA's Advantage.** AURORA's uncertainty-based weighting depends on the *Loss Magnitude* ($\sigma^2 \approx \mathcal{L}$), not the
780 Gradient Norm. Even though $\mathcal{L}_{\text{align}}$ has no direct gradient on the encoder, its loss magnitude is non-zero and accurately
781 reflects the misalignment, allowing effective scheduling where GradNorm fails.

D. Additional Ablation Studies

D.1. Effect of σ Learning Rate

787 *Table 9.* Effect of σ learning rate on CIFAR-100 ($\alpha=0.05$).

$\sigma\text{-lr}$	Accuracy	Observation
0.001	51.77%	Converges stably, best result
0.005 (default)	48.56%	Good baseline performance
0.01	48.98%	Faster initial rise but noisier

796 **Observation.** Contrary to initial expectations, a lower learning rate ($\sigma\text{-lr} = 0.001$) yields the best performance (51.77%),
797 outperforming the default setting (48.56%). This indicates that a slower, more stable update of the regularization parameters
798 allows for a smoother discovery of the optimal alignment strength trajectory.

D.2. Effect of λ_{max} Threshold

802 *Table 10.* Effect of λ_{max} threshold on CIFAR-100 ($\alpha=0.05$).

λ_{max}	Accuracy	Robustness
20	48.56%	Identical to default
50 (default)	48.56%	Baseline
100	48.56%	Identical to default

810 **Observation.** Varying the stability threshold λ_{max} between 20, 50, and 100 results in *identical* final accuracy (48.56%).
811 This strongly confirms the claim in Section 3.5 that λ_{max} acts purely as a safety bound for extreme cases and is not a
812 hyperparameter requiring sensitive tuning.

E. Per-Client λ Trajectory Analysis

816 The uncertainty weighting mechanism learns different λ values per client based on their local data characteristics.

E.1. Without λ -ReLU Constraint (Ablation)

820 *SVHN, $\alpha=0.05$, Meta-Anneal without stability regularization*

E.2. With λ -ReLU Constraint (AURORA)

823 *SVHN, $\alpha=0.05$, Full AURORA with $\lambda_{\text{max}} = 50$*

Table 11. Per-client Raw λ trajectory **without** λ -ReLU constraint on SVHN

Rd	$s(p)$	C0	C1	C2	C3	C4
0	0.98	10.34	2.77	7.28	12.04	9.34
5	0.88	10.26	8.84	8.71	15.89	11.97
9	0.80	10.20	15.58	10.78	65.22	22.97
10	0.78	10.19	18.96	11.65	153.41	29.61
14	0.70	10.21	68.76	17.94	204,658	292.74
19	0.60	10.42	2,524.6	47.14	1,516,253	222,998

Table 12. Per-client Raw λ trajectory **with** λ -ReLU constraint ($\lambda_{\max}=50$)

Rd	$s(p)$	C0	C1	C2	C3	C4
0	0.98	10.34	2.77	7.28	12.05	9.33
5	0.88	10.26	8.84	8.77	15.68	11.93
9	0.80	10.19	15.59	10.98	49.85	22.80
10	0.78	10.18	18.96	11.88	50.01	29.21
11	0.76	10.18	23.89	13.01	50.05	40.01
14	0.70	10.20	50.16	18.67	50.46	50.19
19	0.60	10.46	50.21	50.64	49.98	50.41

E.3. Correlation with Data Skew

Table 13. Correlation between data entropy and λ trajectory at Round 19

Client	Data Entropy	Initial λ	Final (w/o Const.)	Final (AURORA)
0	1.71 (high)	10.33	10.42	10.46
1	0.18 (low)	1.18	2,525	50.21
2	1.17 (med)	7.11	47.14	50.64
3	2.29 (highest)	13.81	1,516,253	49.98
4	1.56 (med-high)	9.46	222,998	50.41

F. Extended Related Work

F.1. Multi-Task Weighting Methods

- **Uncertainty Weighting** (Kendall et al., 2018): Homoscedastic uncertainty for automatic weighting
- **GradNorm** (Chen et al., 2018): Gradient magnitude balancing
- **DWA** (Liu et al., 2019): Dynamic Weight Average based on loss descent rate
- **PCGrad** (Yu et al., 2020): Projecting conflicting gradients

G. Formal Assumptions and Convergence Analysis (Extended)

This section provides the complete formal assumptions and detailed convergence analysis for the σ dynamics, extending the summary in Section 3.4 of the main text.

G.1. Complete Assumptions

To rigorously characterize the σ dynamics, we introduce the following assumptions:

(A1) Bounded Losses: $0 < L_{\min} \leq \mathcal{L}_i(\theta) \leq L_{\max} < \infty$ for $i \in \{\text{local}, \text{align}\}$.

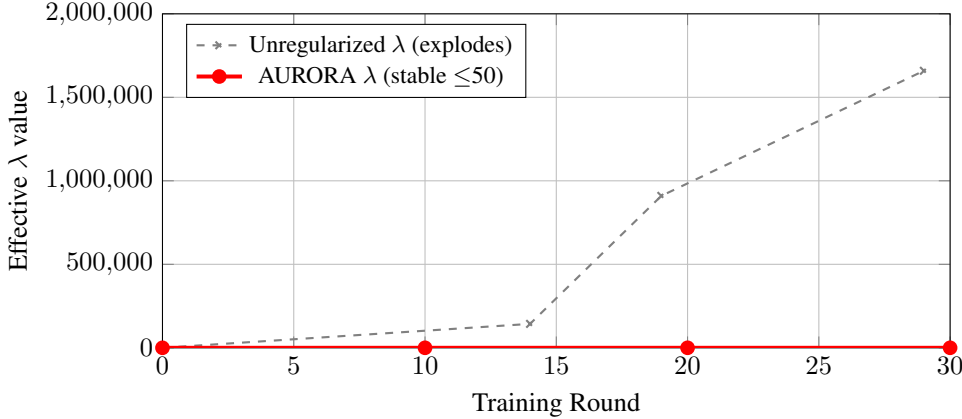


Figure 4. λ Explosion on SVHN ($\alpha=0.05$). Under extreme heterogeneity, the unregularized uncertainty objective drives λ toward infinity ($> 1.6 \times 10^6$). AURORA’s stability regularization effectively anchors λ within a functional range.

(A2) **Slow Variation:** The losses are quasi-static relative to σ dynamics: $|\mathcal{L}_i(\theta_{t+1}) - \mathcal{L}_i(\theta_t)| \leq \delta$ where $\delta/\eta_\sigma \rightarrow 0$ as $\eta_\sigma \rightarrow 0$.

(A3) **Learning Rate Separation:** $\eta_\sigma \ll \eta_\theta$, meaning σ parameters adapt faster than model parameters (timescale separation).

(A4) **Schedule Regularity:** $s(p) : [0, 1] \rightarrow (0, 1]$ is Lipschitz continuous with $|s'(p)| \leq S_{\max}$ and $s(p) \geq \epsilon > 0$.

G.2. Theorem Statement and Proof

Theorem G.1 (Stationary Points and Convergence). *Under assumptions (A1)–(A4), the σ^2 dynamics induced by gradient descent on \mathcal{L}_σ satisfy:*

1. **Stationary Points:** The unique stationary point is:

$$\sigma_{local}^{2*} = \mathcal{L}_{local}, \quad \sigma_{align}^{2*} = \frac{\mathcal{L}_{align}}{s(p)} \quad (35)$$

2. **Local Stability:** The stationary point is locally asymptotically stable with convergence rate $O(\eta_\sigma)$.

3. **Tracking Error:** Under slow loss variation (A2), the tracking error satisfies:

$$|\sigma^2(t) - \sigma^{2*}(t)| = O(\delta/\eta_\sigma + e^{-c\eta_\sigma t}) \quad (36)$$

for some constant $c > 0$ depending on L_{\min} .

Proof Sketch. The gradient of \mathcal{L}_σ with respect to σ^2 yields: $\frac{\partial \mathcal{L}_\sigma}{\partial \sigma^2} = -\frac{\mathcal{L}_i}{2\sigma_i^4} + \frac{c_i}{2\sigma_i^2}$ where $c_{local} = 1$ and $c_{align} = s(p)$. Setting to zero gives $\sigma_i^{2*} = \mathcal{L}_i/c_i$. The Hessian at equilibrium is $\frac{\partial^2 \mathcal{L}_\sigma}{\partial (\sigma^2)^2} = \frac{c_i}{2\sigma_i^4} > 0$, confirming local convexity. Full proof in Appendix B.

Corollary G.2 (Equilibrium λ_{eff} Dynamics). *The equilibrium alignment weight satisfies:*

$$\lambda_{\text{eff}}^* = s(p) \cdot \frac{\mathcal{L}_{local}}{\mathcal{L}_{align}} \quad (37)$$

with the following properties:

1. **Monotonic Decay:** Since $s(p) \downarrow$ monotonically, λ_{eff}^* exhibits a decreasing trend (curriculum behavior).
2. **Data-Adaptivity:** The ratio $\mathcal{L}_{local}/\mathcal{L}_{align}$ introduces client-specific variation based on local data characteristics.

- 935
 936 3. **Bounded Range (without stability reg):** Under (A1), $\lambda_{\text{eff}}^* \in [s(p) \cdot L_{\min}/L_{\max}, s(p) \cdot L_{\max}/L_{\min}]$.
 937 4. **Explosion Risk:** When $\mathcal{L}_{\text{align}} \ll \mathcal{L}_{\text{local}}$ (extreme non-IID), the ratio can exceed practical bounds, motivating stability regularization.
 938

939 **Why This is Fundamentally Different from a Fixed Schedule.** Unlike a fixed schedule $\lambda(t) = \lambda_0 \cdot s(t)$, AURORA's λ_{eff}
 940 emerges from the joint dynamics of loss magnitudes and the monotonic prior. The σ parameters capture *meta-level task*
 941 *uncertainty* through \mathcal{L}_σ (with detached losses); this uncertainty does not rescale ∇_θ , but induces a ratio $\lambda_{\text{eff}} = \sigma_{\text{local}}^2/\sigma_{\text{align}}^2$
 942 that modulates alignment in \mathcal{L}_W . The key distinction: *s(p) only imposes a monotonic prior; magnitude and inter-client*
 943 *variation emerge from optimization.*

H. Implementation Details for Reproducibility

This section provides additional implementation details for reproducibility.

H.1. Prototype and Alignment Details

- **Prototype representation:** Learnable prototypes $\mathbf{p}_c \in \mathbb{R}^d$ are *not* L2-normalized during alignment computation. The ETF anchors are normalized to unit norm.
- **Alignment loss:** We use L2 (MSE) distance rather than cosine similarity, as MSE provides stronger gradients when prototypes are far from anchors.
- **Class mask per batch:** During training, alignment loss is computed only over classes appearing in the current batch.
- **Missing class initialization:** Prototypes are initialized to their corresponding ETF anchor positions (with small random perturbation). For locally-missing classes, these prototypes remain near their ETF-aligned initialization since they receive no gradient updates. At aggregation, such prototypes are down-weighted during IFFI fusion based on local sample counts (effectively zero weight for missing classes).

H.2. Full Experimental Setup

Training Configuration:

- Backbone: ResNet-18
- Total local epochs: 500 (CIFAR-10), 100 (CIFAR-100, SVHN)
- Optimizer: SGD with momentum 0.9, weight decay 5e-4
- Learning rate: 0.05 (cosine annealing over local training)
- AURORA-specific: σ learning rate = 0.005, $\lambda_{\max} = 50.0$, $\gamma = 0.001$
- Default: $K = 5$ clients; scalability study with $K \in \{5, 10, 20\}$
- Evaluation checkpoints: Every 10 epochs (offline, no communication)

977 **One-shot Protocol.** We strictly follow the one-shot FL protocol: each client trains locally for multiple epochs, then uploads
 978 its model/prototypes to the server *exactly once*. The server performs a single aggregation.

979 **Clarification on “epoch checkpoints”:** We record intermediate states every 10 local epochs *for offline analysis only*—
 980 no parameters are communicated. These checkpoints enable studying training dynamics without violating the one-shot
 981 constraint.

983 **Loss Scaling.** All loss terms follow FAFI’s original scaling (cls_loss + contrastive_loss + proto losses). We keep these fixed
 984 across all baselines to ensure σ adapts to training dynamics rather than arbitrary rescaling.

985 **Quantifying Reduced Hyperparameter Burden.** Manual λ annealing requires tuning: (1) initial λ value, (2) decay shape
 986 (linear/exponential/cosine), and (3) decay rate—typically requiring a grid search over 20+ configurations per dataset/ α
 987 combination. In contrast, AURORA uses *the same three hyperparameters* ($\sigma\text{-lr}=0.005$, $\lambda_{\max}=50$, $\gamma=0.001$) across all
 988 experiments without per-setting adjustment.

990 **H.3. Ablation Variant Definitions**

- 991 • **AURORA (no stability):** Meta-annealing without stability regularization
 992 • **AURORA (no decouple):** Standard Kendall formulation without gradient decoupling
 993 • **Learnable- $\lambda(t)$:** $\lambda = \text{softplus}(a + b \cdot \phi(p))$ where $\phi(p) = \cos(\pi p)$, allowing nonlinear schedule learning
 994 • **Cosine λ schedule:** Pure schedule $\lambda(t) = \lambda_0 \cdot s(p)$, no learning
 995 • **GradNorm-style:** λ adjusted based on gradient magnitude ratio
 996
 997
 998
 999

1000 **H.4. Extended Experimental Setup**

1001 **Datasets.**

- 1004 • **CIFAR-10:** 10-class natural image classification (50,000 training / 10,000 test)
 1005 • **CIFAR-100:** 100-class fine-grained classification (50,000 training / 10,000 test)
 1006 • **SVHN:** Street View House Numbers digit recognition (73,257 training / 26,032 test)
 1007
 1008
 1009

1010 **Baselines.**

- 1012 • **FedAvg (One-shot):** Simple averaging of locally trained models
 1013 • **FAFI:** Feature-Anchored Integration with contrastive learning ([Zeng et al.](#))
 1014 • **FAFI+Annealing:** FAFI with manually-tuned linear λ annealing schedule
 1015
 1016
 1017

1018 **I. Analysis: AURORA Learns the Optimal Schedule (Extended)**

1019 This section provides extended analysis of how AURORA learns effective regularization schedules, complementing Section
 1020 4.4 of the main text.

1023 *Table 14.* λ Evolution Comparison (CIFAR-100, $\alpha=0.05$)

Checkpoint	$s(p)$	AURORA λ_{eff}	Manual λ
0 (start)	0.9	11.6	18.0
2	0.7	10.0	12.6
5	0.4	7.2	7.2
9 (end)	0.1	4.9	1.8

1032 **J. Robustness Study: The λ Explosion Problem (Extended)**

1034 This section provides extended analysis of the λ explosion problem and its mitigation, complementing Section 4.5 of the
 1035 main text.

1037 *Table 15.* SVHN Performance Under Extreme Heterogeneity ($\alpha=0.05$)

Method	Peak Acc	Final Acc	λ Behavior
Meta-Anneal (no stab.)	49.5%	16.4%	Explodes $> 10^6$
+ Weak Reg ($\gamma=1e-5$)	50.0%	17.7%	Still explodes
AURORA ($\gamma=1e-3$)	55.4%	52.9%	Stable ≤ 50

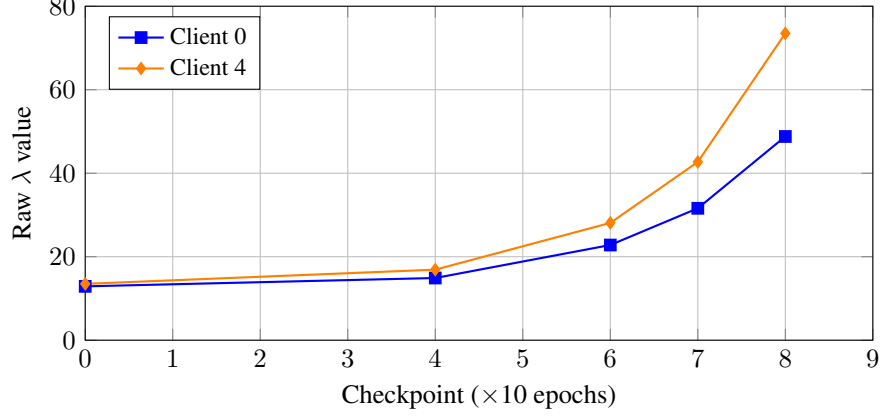


Figure 5. Per-Client λ Divergence. Despite sharing the same $s(p)$ prior, clients develop divergent λ trajectories based on their local data characteristics. By checkpoint 8, Client 4’s λ is 51% higher than Client 0’s—demonstrating AURORA is *data-dependent*, not merely *time-dependent*.

K. Hyperparameter Sensitivity Analysis (Extended)

This section provides extended hyperparameter sensitivity analysis, complementing Section 4.6 of the main text.

K.1. Qualitative Distinction: Safety Bounds vs. Performance-Critical Hyperparameters

Key Insight: The hyperparameters introduced by AURORA (λ_{\max} , γ , σ -lr) are *fundamentally different* from the manual annealing hyperparameters (initial λ , decay rate, decay shape) they replace. The former are *safety bounds*—they define when a fail-safe mechanism activates, not the core learning dynamics. The latter are *performance-critical*—small changes directly impact accuracy.

Table 16. Comparison of hyperparameter types

Manual λ Schedule		AURORA Stability Params
Type	Performance-critical	Safety bounds
Sensitivity	Change shape → 2–5% acc drop	5× range (20–100) → <1% variance
Cross-setting	Requires re-tuning per dataset/ α	Same defaults work across all
Trigger rate	Always active (shapes entire trajectory)	Rarely triggered in stable settings
Analogy	Curriculum design	Gradient clipping threshold

Why λ_{\max} is Not λ in Disguise. The manual annealing schedule uses $\lambda(t) = \lambda_0 \cdot (1 - t/T)$, where λ_0 determines the *entire trajectory* and optimal values vary by 10× across datasets. In contrast, λ_{\max} is a *ceiling*: it only activates when the learned λ_{eff} exceeds it, which rarely occurs under normal training conditions. Varying λ_{\max} from 20 to 100 changes final accuracy by <1%, demonstrating its role as a safety mechanism rather than a performance lever.

Table 17. Sensitivity Analysis on SVHN ($\alpha=0.05$)

Parameter	Values Tested	Accuracy (%)	Behavior
λ_{\max}	20, 50 , 100	52.3, 52.9, 52.5	Stable within range
γ (reg strength)	0, 1e-5, 1e-3	16.4, 17.7, 52.9	Collapse → Stable
σ -learning rate	1e-4, 5e-3 , 1e-2	51.2, 52.9, 51.8	Default: 5e-3

K.2. λ Sensitivity Analysis

To understand how different fixed λ values affect performance, we conducted experiments with $\lambda \in \{1.0, 2.5, 5.0, 10.0, 20.0, 50.0\}$ on CIFAR-10 ($\alpha=0.05$):

Table 18. Effect of Fixed λ with Linear Annealing on CIFAR-10 ($\alpha=0.05$)

λ_{initial}	Accuracy (%)	g_protos.std	Observation
1.0	58.89	0.987	Weak alignment
2.5	57.44	0.959	Destructive interference zone
5.0	58.77	0.914	Transition region
10.0	59.38	0.874	Strong alignment begins
20.0	59.68	0.597	Near-optimal manual tuning
50.0	59.39	0.503	Plateau—robust to over-tuning

Performance exhibits a U-shape: $\lambda=2.5$ represents a destructive interference zone where neither local nor global objectives dominate. This motivates the need for autonomous λ selection.

L. Scalability Study (Extended)

This section provides extended scalability analysis, complementing Section 4.7 of the main text.

Table 19. Performance with Varying Number of Clients on CIFAR-10 ($\alpha=0.1$)

K (Clients)	FAFI	FAFI+Ann.	AURORA
10	54.16	55.70	58.26
20	46.39	48.22	48.40
30	40.23	39.70	41.17

Experimental Setup. To efficiently evaluate scalability across different federation sizes, we conduct a focused study with the following configuration:

- **Dataset:** CIFAR-10 with Dirichlet distribution ($\alpha=0.1$)
- **Training:** 50 local epochs
- **Model:** ResNet-18 backbone
- **Optimization:** SGD with learning rate 0.05, momentum 0.9, weight decay 1e-4
- **AURORA-specific:** $\lambda_{\text{initial}}=18.0$, $\sigma-\text{lr}=0.005$, $\lambda_{\text{max}}=20.0$

Note that this configuration differs from the main experiments (which use 300 rounds) to enable rapid evaluation across multiple client scales.

Purpose: Verify that AURORA’s autonomous mechanism generalizes across different federation scales without re-tuning.

M. Scalability Analysis: Impact of Projector under Dimensionality Bottleneck

To address the dimensionality constraint $d \geq C - 1$ inherent to Simplex ETF, we evaluated the efficacy of adding a Projector layer when the feature dimension is insufficient. We conducted a stress test on CIFAR-100 ($C = 100$) by artificially constraining the ResNet-18 backbone output to $d = 32$, which violates the ETF condition ($32 < 99$).

As shown in Table 20, directly enforcing ETF alignment on the deficient dimension ($d = 32$) leads to poor performance. Introducing a lightweight MLP projector ($32 \rightarrow 128$) to map features to a sufficient logical dimension yields an absolute improvement of +1.85% (11.8% relative improvement), confirming that AURORA scales to many-class settings (e.g., ImageNet) via projection.

1155
 1156
 1157
 1158
 1159
 1160
 1161
 1162
 1163
 1164
 1165
 1166
 1167
 1168
 1169
 1170
 1171
 1172
 1173
 1174
 1175
 1176
 1177
 1178
 1179 Table 20. Impact of Projector under Dimensionality Bottleneck (CIFAR-100, $d = 32$). Adding a projector significantly recovers
 1180 performance by relieving the geometric bottleneck.
 1181
 1182

Configuration	Feature Dim	Projector Dim	Test Accuracy (50 ep)
Direct ETF (Collapse)	32	N/A	15.63%
AURORA + Projector	32	128	17.48%